Advances in Military Technology
Vol. 21, No. 1, 2026, pp. 51-66
ISSN 1802-2308, eISSN 2533-4123
DOI 10.3849/aimt.02002

Study on the Influence of Edge-Thickness Liner on Explosively Formed Projectiles

D. Thanh Tran, V. Minh Do, H. Quan Pham*, and X. Son Bui

Faculty of Special Equipment, Le Quy Don Technical University, Hanoi, Vietnam

The manuscript was received on 9 June 2025 and was accepted after revision for publication as an original research paper on 11 March 2026.

Abstract:

This study investigates the effect of liner thickness distribution, expressed as the edge-to-apex ratio (δ_2/δ_1), on the formation and performance of explosively formed projectiles (EFP). Numerical simulations and experimental tests were conducted to assess key parameters such as velocity, projectile shape, flight stability, and penetration depth. Results show that low δ_2/δ_1 ratios lead to blunt, large-diameter projectiles with poor aerodynamic properties, while high ratios produce slender shapes that often develop hollow tails, reducing stability and penetration. The most effective performance was achieved at moderate δ_2/δ_1 values (around 0.4–0.6), where a favorable balance between collapse dynamics, shape, and mass distribution resulted in improved flight behavior and terminal effectiveness. These insights are useful for optimizing EFP warhead design.

Keywords:

explosively formed projectile, thickness liner, penetration, Ansys Autodyn

1 Introduction

Explosively formed projectiles (EFP) are precision munitions designed to destroy armored targets at stand-off distances by reshaping a metal liner into a high-velocity slug upon detonation. The liner's geometry, particularly the thickness variation from top to edge, critically influences the projectile's velocity, stability, and penetration performance. An optimized design ensures uniform velocity, minimizes fragmentation, and enhances both flight stability and terminal effectiveness.

The penetration ability of an EFP against armored targets can range from 0.3 to 1 time the warhead caliber [1, 2]. By adjusting design parameters such as the liner radius, outer radius, and the position of the liner's center, different liner shapes can be created. These changes affect the EFP formation process, allowing the production of

* *Corresponding author: Faculty of Special Equipment, Le Quy Don Technical University, Hoang Quoc Viet 236, Hanoi, Vietnam. Phone: +84 862 48 64 18, E-mail: phquanstudying@lqdtu.edu.vn*

both forward and reverse EFPs, which influence the projectile's penetration performance and effective range. Many researchers have investigated how different liner designs affect the formation and penetration capability of EFPs against steel targets. Wu introduced an early design for the liner used in explosively formed projectile (EFP) warhead [3]. Salkičević suggested reducing the liner thickness from 6 to 4 mm to increase the speed and penetration ability of the projectile [4]. Cardoso studied liners with changing thickness from top to edge and found that they created faster projectiles than liners with the same thickness throughout [5]. Yang and colleagues examined how the shape of the liner affects the way the EFP forms and how well it penetrates targets [6]. Couque and Hussain ran experiments and advised using Ansys Autodyn software with the Modified Johnson-Cook (MJC) model, which gives more accurate results than the regular Johnson-Cook (JC) model [7-9]. Yuan performed simulations and tests on EFPs with polygon-shaped shells to improve projectile design by adding fins [10].

However, the influence of liner thickness at the edge on EFP formation and its penetration into steel targets has not been thoroughly investigated through simulations or experiments. This paper aims to investigate the EFP formation process, key parameters, velocity distribution, and interaction with steel targets using liners of different heights. Numerical simulations were performed using Ansys Autodyn 2D software. In addition, experiments were carried out using the same warhead configurations as in the simulations. The experimental results are analyzed and compared with the simulation outcomes.

2 Simulation Model and Material Model

2.1. Geometric Model and Calculation Method

This study focuses on a 54 mm EFP warhead, as illustrated in Fig. 1. The warhead comprises four primary components: casing, explosive charge, detonator, and liner. The liner is hemispherical, made of CU-OFHC copper (Copper – Oxygen-Free High Conductivity), and characterized by its height h, diameter d, outer radius r_1, inner radius r_2, top thickness δ_1, and edge thickness δ_2. The positions of the centers of curvature for r_1 and r_2 along the axis of symmetry are defined by distances X_1 and X_2 from the warhead base, respectively. The casing is made of polyethylene and has a cylindrical shape with outer diameter D, length L, wall thickness t_1, and base thickness t_2. The explosive charge, composed of C4, is contained within the casing and has the same diameter d and height l.

To determine the structural parameters for the study, in addition to the fixed values of the charge diameter D and liner diameter d, some initial input parameters must be selected. According to references [3, 5], a liner with thickness gradually changing from the top to the edge produces higher EFP velocity and deeper penetration compared to a liner with uniform thickness. Currently, there are no studies focusing on the effect of liner thickness at the mouth region in shaped charge warheads. Therefore, this paper investigates the impact of varying top thickness within the range of $(0.3 \div 1)\ \delta_1$ for further analysis. The parameters of the structural configurations are listed in Tab. 1.

The formation of the explosively formed projectile and its interaction with steel targets were simulated using Ansys Autodyn software. The projectile parameters obtained from the formation stage were used as input conditions for the penetration

analysis. To take advantage of axial symmetry and to reduce computational time, a two-dimensional symmetric model was employed. The casing, liner, explosive, and surrounding air were all modeled using a Eulerian mesh with a uniform cell size of 0.25×0.25 mm. Flow out boundary conditions were applied on all outer boundaries of the computational domain, except along the axis of symmetry. The overall simulation setup, including geometry definition, mesh refinement, material selection, and placement of diagnostic gauges, was carried out within the Autodyn two-dimensional environment based on procedures described in prior research [6, 9-12].

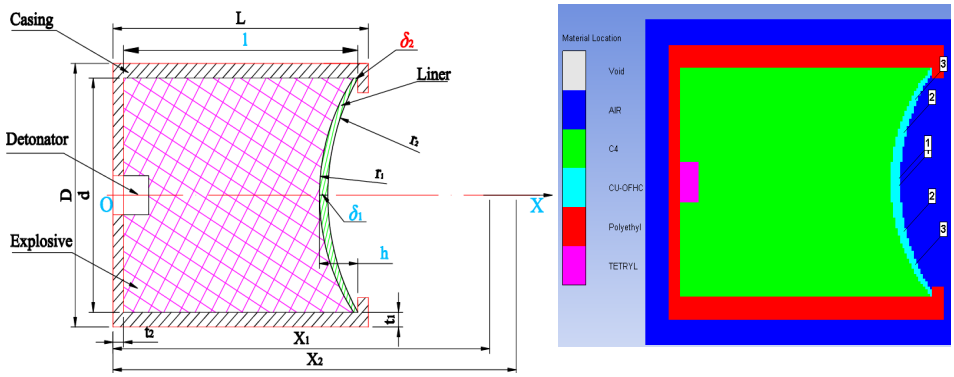

Fig. 1 EFP warhead model and simulation model in Autodyn

Tab. 1 Parameters of EFPW with varying edge liner thickness

Size	Unit	Type							
		1	2	3	4	5	6	7	8
D	mm	54.00							
d	mm	45.20							
L	mm	59.24							
l	mm	54.24							
t_1	mm	2.50							
t_2	mm	4.40							
h	mm	9.04							
δ_1	mm	2.00							
X_1	mm	90.26							
r_1	mm	39.80							
δ_2	mm	0.6	0.8	1	1.2	1.4	1.6	1.8	2
X_2	mm	82.94	83.57	84.24	84.95	85.71	86.51	87.35	88.26
r_2	mm	34.48	35.11	35.78	36.49	37.25	38.05	38.89	39.8
δ_2/δ_1		0.3	0.4	0.5	0.6	0.7	0.8	0.9	1

2.2. Material Model and Parameters

The plastic explosive C4 is modeled as an ideal elastoplastic material that obeys the von Mises yield criterion. Upon detonation, C4 transforms into a high-pressure gas, and its behavior is described by the Jones Wilkins Lee equation of state. In this model, the pressure of the detonation products p is expressed as a function of the relative volume V and the specific internal energy E, capturing the rapid expansion and high-energy release characteristics of the explosive.

$$p = A\left(1-\frac{\omega}{R_1 V}\right)\mathrm{e}^{-R_1 V} + B\left(1-\frac{\omega}{R_2 V}\right)\mathrm{e}^{-R_2 V} + \frac{\omega E}{V} \tag{1}$$

where ω, A, B, R_1, R_2 are the experimental constants, with values in Tab. 2 [6-8].

Tab. 2 Values of the parameters in the JWL equation for the state of C4 explosive

Parameters	Unit	Value
ρ	kg/m^3	1601
A	kPa	6.0977×10^8
B	kPa	1.2950×10^7
R_1	—	4.5
R_2	—	1.4
ω	—	0.25
D	m/s	8 193
E	kJ/m^3	9.000001×10^6

The warhead casing is constructed from polyethylene plastic. When subjected to explosive loading, the material experiences substantial volumetric expansion and shape deformation. To accurately represent this behavior, the shock equation of state is applied. The model parameters are determined from experimental data, with specific values listed in Tab. 3.

Tab. 3 Values of the parameters in the Shock equation for the polyethylene plastic

Parameters	Unit	Value
ρ	kg/m^3	915
Γ	—	1.64
C_1	m/s	2 901
S_1	—	1.481
C_2	m/s	0
S_2	—	0

The liner is typically made of Cu-OFHC copper and is modeled using the modified Johnson Cook elastic plastic constitutive model. This model captures strain hardening, strain rate sensitivity, and thermal softening effects, making it suitable for simulating high strain rate deformation during EFP formation [6-8].

$$\sigma = \left(A + B\varepsilon_{\mathrm{p}}^{n}\right)\left[1 + C\ln\frac{\varepsilon^{*}}{\varepsilon_{\bullet}^{*}} + D\left(\frac{\varepsilon^{*}}{\varepsilon_{1}^{*}}\right)^{k}\right]\left[1 - \left(\frac{T - T_{\mathrm{ref}}}{T_{\mathrm{melt}} - T_{\mathrm{ref}}}\right)^{m}\right] \tag{2}$$

in which: σ – the dynamic yield stress; *A, B, C, D n*, *m* and *k* are the constants of the material determined experimentally; ε_{p} – the plastic strain; ε^{*} – the plastic strain rate; $\varepsilon_{\bullet}^{*}$ – the reference value for plastic strain rate; ε_{1}^{*} – the reference strain rate characterizing the transition between thermally activated and viscous regime; T – the instantaneous temperature; T_{ref} – the initial temperature; T_{melt} – the melting temperature of the material. In this simulation, the liner is composed of CU-OFHC copper and modelled using a Modified Johnson-Cook (MJC) model. To ensure numerical stability during high strain rate deformation in the range of 10^3 to 10^6 per second, the hardening constant of the copper liner increased by 10 %, from 29.2 GPa to 32.1 GPa. This adjustment helps prevent premature plastic instability during the intense loading phase of EFP formation. The steel target, made from Steel 1006, is modeled using the standard Johnson Cook constitutive model, which effectively captures strain hardening, strain rate sensitivity, and thermal softening. The corresponding material parameters for both the liner and the target are provided in Tab. 4.

To describe the equation of state of air in mathematical simulation, we use the gamma form of equation of state:

$$p = \rho(\gamma - 1)E \tag{3}$$

where γ= 1.4, ρ = 1.225 kg/m^3, E =2.5 × 10^5 J/kg [13].

During the penetration phase, a Lagrangian mesh is applied to both the EFP and the target to accurately capture material deformation and failure. The EFP parameters used in this stage are obtained from the earlier formation simulation based on the Eulerian method. The target is modeled as a Steel 1 006 plate with a width of 200 millimeters and a thickness of 30 millimeters. Its behavior under high strain and impact is defined by the shock equation of state for pressure response, and by the Johnson-Cook model for strength and failure characteristics with D_1, D_2, D_3, D_4, D_5 as failure parameters given in Tab. 5 [14].

Tab. 4 Parameter values in the elastic-plastic model

Parameters	**Unit**	**Value**	
		CU-OFHC	**Steel 1006**
Equation of state	—	Linear	Shock
Density	kg/m^3	8 960	7 830
Melting temperature	K	1 356	1 811
Strength model	—	JC	JC
Yield stress *A*	GPa	0.09	0.35
Hardening constant *B*	GPa	0.3212	0.275
Strain rate constant *C*	—	0.025	0.022
Hardening exponent *n*	—	0.31	0.36
Thermal softening exponent *m*	—	1.09	1

DOI 10.3849/aimt.02002

Tab. 5 Values of Johnson-Cook failure model parameters

D_1	D_2	D_3	D_4	D_5
0.05	4.22	–2.73	0.0018	0.55

The simulation model of the impact interaction between the EFP and the steel target is illustrated in Fig. 2. Both the projectile and the target are discretized using uniform rectangular elements with a mesh size of 0.2 millimeters, ensuring sufficient resolution to capture detailed deformation and failure during penetration.

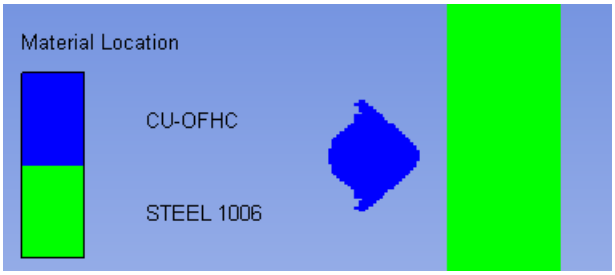

Fig. 2 Simulation of EFP impact on steel plate

3 Experimental Setup and Validation

The numerical simulation results of the formation and penetration process of EFP were confirmed by experimental methods. The simulation and experimental results, including the velocity and structural shape of EFP, were compared. For the penetration process of EFP, the hole diameter and penetration depth after impacting on a 20 mm thick steel target were compared.

3.1 Explosively Formed Projectiles and Experimental Target

The liner configuration with Type 3 and Type 8 was selected for experimental validation, with its geometry and dimensions presented in Tab. 1. The forming liner is made from Cu-OFHC copper, while the casing is composed of polyethylene plastic. The explosive charge is C4 plastic explosive, initiated by a No. 8 electric detonator. The target is made of 45# steel, with a plate size of 20 mm in thickness, and 500 mm in both width and length, as illustrated in Fig. 3.

Fig. 3 EFP Warhead and steel target

3.2 Experimental Setup

The experimental setup for measuring the velocity and penetration performance of the EFP is illustrated in Fig. 4. The tested EFP warhead is mounted in a horizontal orientation, and a 45# steel target plate with a thickness of 20 mm is positioned at a standoff distance of 3 meters. To capture the projectile velocity, an electronic timer (UTC-8 model) is placed 2 meters from the EFP warhead along its flight path. After impact, the diameter and depth of the penetration cavity on the steel plate are measured to evaluate the terminal performance of the projectile.

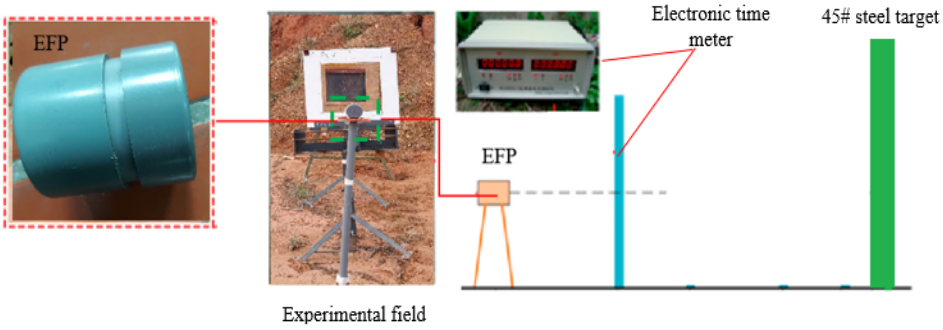

Fig. 4 Experimental measurement of EFP velocity and penetration depth

3.3 Experimental Results

After the static blasting of the test symbols, the dimensions of the through hole on the steel plate were measured to determine its diameter and depth, as shown in Fig. 5.

Symbol 0.1 Symbol 0.2 Symbol 3.2

Fig. 5 Experimental results

The results of EFP velocity (V), hole width (W_h) and hole depth (D_h) when tested for each type of EFP with different edge thickness are shown in Tab. 6,

Tab. 6 EFP velocity and penetration results on steel target

	Type 3			**Type 8**		
Symbol	**0.1**	**0.2**	**0.3**	**3.1**	**3.2**	**3.3**
V [m/s]	2 278	2 150	1 859	1 865	1 696	1 788
V_{Ag} [m/s]	2 096			1 783		
W_h [mm]	36	37	40	28	25	26
$W_{h.Ag}$ [mm]	37.7			26.3		
D_h [mm]	20	20	18	17	14	16

In which type 3 has symbols 0.1, 0.2, 0.3 and type 8 has symbols 3.1, 3.2, 3.3 and are tested in order of numbering from smallest to largest.

4 Results and Discussion

Tab. 7 presents the results of the analysis on how the edge thickness liner affects the formation of explosively formed projectiles at t = 0.7 m/s. The evaluation was conducted across all warhead configurations listed in Tab. 1, providing a comparative basis for understanding the influence of liner geometry on projectile shape, velocity, and kinetic energy during the early formation stage.

4.1. Shape of EFP

The shape and aerodynamic behavior of EFP are strongly influenced by the collapse and deformation of the liner, which is in turn governed by the edge thickness as shown in the simulation results in Tab. 7. The findings of this study are consistent with the published literature on EFP [3, 6]:

Type 1 produces a solid, blunt, wide-diameter EFP with poor aerodynamic characteristics. This configuration results in a significant loss of velocity during flight due to high drag.

Types 2–4 produce EFP with a solid shape and good aerodynamic configuration. These EFPs exhibit stable flight and slow down over distance, indicating efficient aerodynamic behavior. However, Type 4 begins to exhibit a small hollow tail, which may adversely affect flight stability and penetration performance.

Types 5–8 continue to produce aerodynamically shaped EFP, but with increasingly large and pronounced hollow tails. These hollow regions reduce flight stability and significantly reduce the EFP's penetration ability.

Therefore, the projectile shapes formed from Types 2 to 4 offer the best combination of penetration performance and flight stability. These designs produce projectiles that are not only effective upon impact but also maintain their intended trajectory.

Tab. 7 Shape and dynamic parameters of EFP

Time [ms]		0.1	0.3	0.5	0.7
Type 1 V_{EFP} = 2040 m/s E_{kin}= 37.94 kJ					
	Displacement [mm]	252	668	1 081	1 490
Type 2 V_{EFP} = 2010 m/s E_{kin}= 38.63 kJ					
	Displacement [mm]	249	658	1 064	1 468
Type 3 V_{EFP} = 1982 m/s E_{kin}= 39.03 kJ					
	Displacement [mm]	246	649	1 050	1 448
Type 4 V_{EFP} = 1956 m/s E_{kin}= 39.45 kJ					
	Displacement [mm]	243	639	1 033	1 426
Type 5 V_{EFP} = 1929 m/s E_{kin}= 39.26 kJ		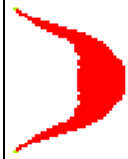			
	Displacement [mm]	241	631	1 019	1 406

Type 6 V_{EFP} = 1912 m/s E_{kin}= 38.76 kJ	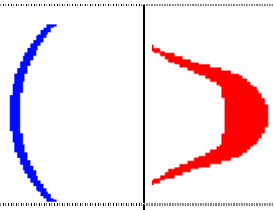				
	Displacement [mm]	239	624	1 008	1 391
Type 7 V_{EFP} = 1889 m/s E_{kin}= 38.45 kJ	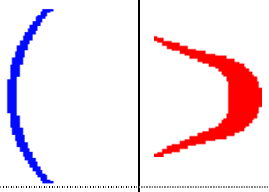				
	Displacement [mm]	238	618	1 001	1 376
Type 8 V_{EFP} = 1840 m/s E_{kin}=38.12 kJ	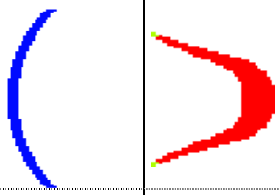				
	Displacement [mm]	236	612	986	1 359

4.2. Velocity of EFP

The velocity of the EFP is a crucial factor in determining its ability to reach and penetrate the target effectively. In this study, projectile velocity clearly depends on the thickness ratio between the edge and the apex of the liner. When the edge of the liner is relatively thin, as observed in the Type 1 configuration, the liner collapses more rapidly and uniformly. This results in the highest projectile speed, approximately 2 040 m/s.

As the thickness at the liner's edge increases, moving progressively through Types 2, 3, and 4, the velocity decreases in a gradual and predictable manner. For example, the projectile velocity in Type 4 drops to around 1 956 m/s, which represents a reduction of more than 4 % compared to the initial configuration. The thicker edge adds resistance to the collapse process, slowing down the convergence of the liner material toward the projectile tip.

When the edge becomes significantly thicker, as in Type 5 through Type 8, the loss in velocity becomes more pronounced. In the configuration with the thickest liner edge, Type 8, the projectile speed reduces to 1 840 m/s. This marks a decline of nearly 10% from the maximum value achieved in Type 1. These findings show that although thicker liners contribute additional mass, they also hinder the collapse dynamics, resulting in reduced projectile velocity, as seen in the results in Fig. 6. The most

effective performance in terms of velocity is found in configurations with moderate edge thickness, particularly from Type 2 to Type 4.

4.3. Kinetic Energy of EFP

Kinetic energy reflects the combination of both projectile mass and velocity. A fast-moving projectile with low mass may carry less energy than a slower, heavier one. In the case of Type 1, although the projectile reaches the highest speed, its relatively light mass limits the kinetic energy to around 37.94 kJ.

As the edge of the liner becomes slightly thicker in Types 2, 3, and 4, the projectile mass increases, and the kinetic energy rises accordingly. Among these, Type 4 achieves the highest energy level at approximately 39.45 kJ, which is about 4 % higher than that of Type 1. This suggests that there is a favorable balance between mass gain and acceptable velocity reduction in the mid-range configurations.

However, once the edge thickness continues to increase beyond this point, the decreasing velocity begins to outweigh the benefit of added mass. From Type 5 onward, the kinetic energy begins to decline gradually. By the time it reaches Type 8, the kinetic energy falls to approximately 38.12 kJ, which is about 3.4 % below the peak value observed in Type 4. These results indicate that while increasing edge thickness can initially improve energy transfer, excessive thickening leads to a loss in overall efficiency.

Thus, the most optimal kinetic performance is found in the mid-range configurations, especially those between Type 2 and Type 4, where mass and speed are best balanced, as shown in Fig. 6.

4.4. Penetration Process

After formation, the explosively formed projectile impacts the 45# steel target plate, which has a thickness of 30 millimeters. As shown in Fig. 7, the target material undergoes deformation primarily through compressive and shear stresses, which represent the dominant failure mechanisms during the interaction. A combined tensile and compressive stress zone is observed at both the front and rear surfaces of the target plate. As the penetration depth increases, the tensile stress zone becomes more prominent, particularly at the edge of the shear-affected region, due to substantial material elongation. The reflection of transverse stress waves from the rear surface, together with the continuous advancement of the projectile, further contributes to the propagation of target damage. In general, two distinct zones are identified during the penetration process: a compressive zone located near the front surface where the material is primarily compressed, and a tensile zone near the rear surface where the material experiences tensile failure. As penetration progresses, resistance to the projectile increases, leading to an expansion of the damage zone.

The simulation results when EFP penetrates the steel plate for hole diameters b and penetration depths p with different the edge thickness liners are shown in Fig. 8.

Penetration depth is one of the most direct indicators of an EFP's effectiveness against a target. The results show that penetration depth is strongly influenced by the geometry of the liner. Among the eight designs, Type 2 produces the deepest penetration. This suggests that a moderately thin edge combined with high projectile velocity allows for efficient forward momentum and concentrated impact.

DOI 10.3849/aimt.02002

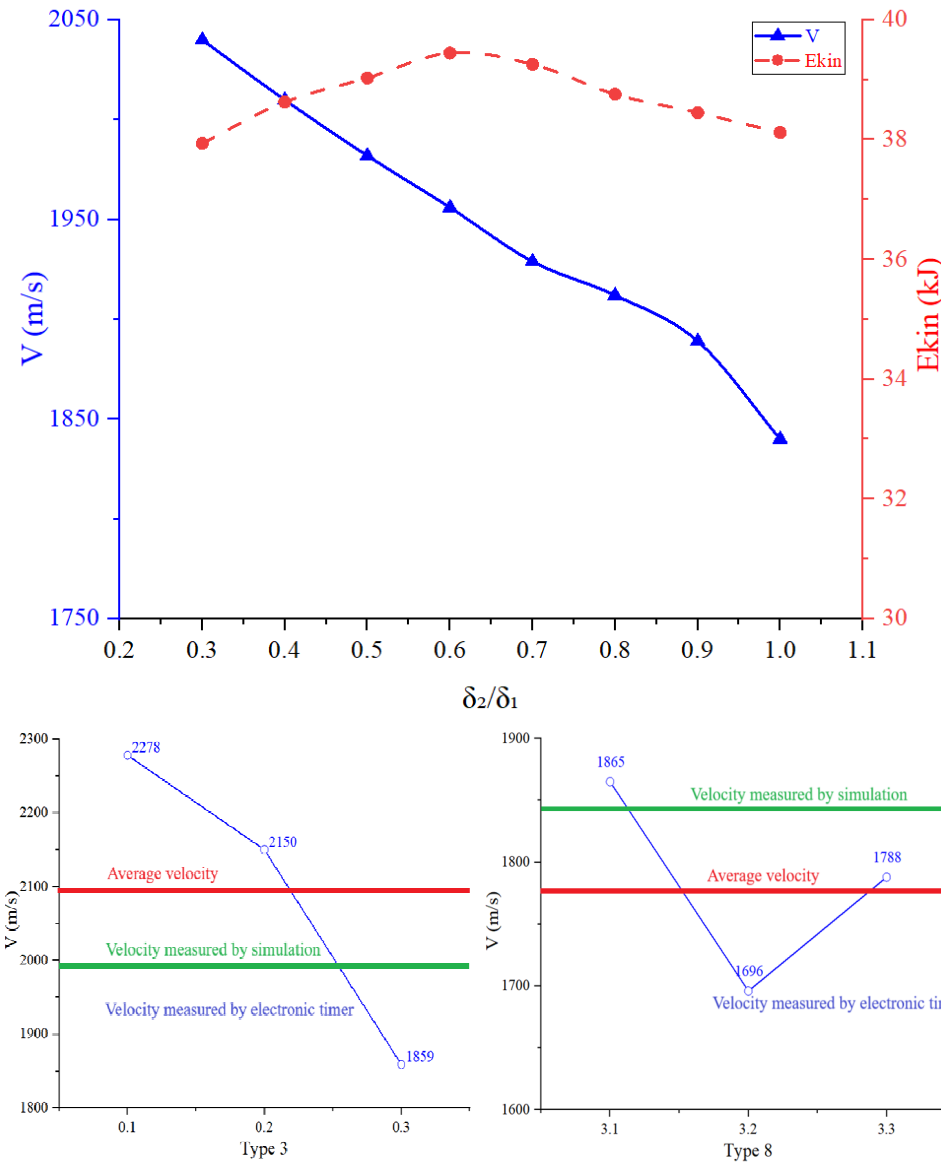

Fig. 6 Effect of the edge thickness liner on EFP velocity and kinetic energy obtained by simulation and experiments

Both Type 1 and Type 3 also achieve comparable penetration depth, with only small differences. These configurations maintain a good shape during collapse and ensure focused delivery of energy into the target. However, when the liner edge becomes thicker, starting from Type 4, a gradual reduction in penetration depth is observed.

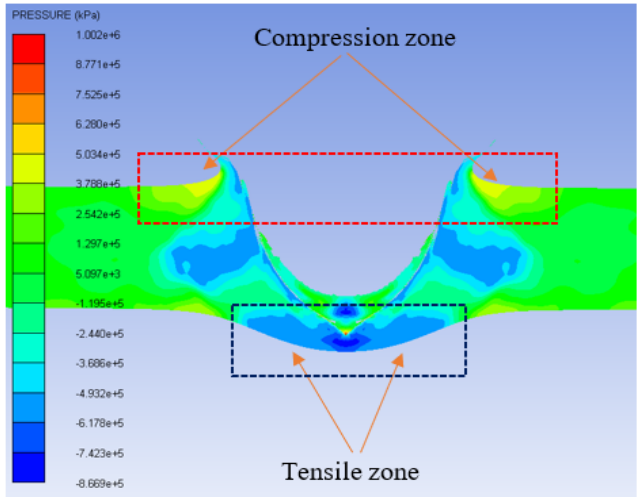

Fig. 7 Steel plate subjected to EFP loading

In Type 7 and especially Type 8, where the edge thickness is highest, the projectile becomes shorter and less streamlined. This results in a significant decrease in penetration capability. Compared to Type 2, the reduction in penetration depth exceeds 30 %, highlighting the negative impact of excessive liner edge thickness on target perforation.

The cavity width reflects the size of the hole left on the surface of the target after impact and provides insight into the projectile's lateral damage capability. Among the eight configurations, Types 3 and 4 create the widest impact cavities. These designs produce projectiles with broader heads and stable geometry, leading to better distribution of kinetic energy across a wider surface area.

In contrast, Type 1, which forms a narrow and sharp projectile, results in a smaller cavity despite its high speed. As the liner edge becomes thicker in the later configurations, the projectile shape becomes more compact and blunter. Although the mass increases, the shape limits lateral expansion and reduces the overall cavity width.

In Types 7 and 8, the projectile forms are less aerodynamic and slower, leading to the narrowest cavity widths among all the tested cases. This shows that a heavier projectile does not necessarily cause more damage if its shape and speed are compromised.

4.5 Experimental Validation

To evaluate the accuracy of the simulation results, experimental tests were conducted for two representative liner configurations: Types 3 and 8, as illustrated in Fig. 8. These two cases represent a high-performance mid-range geometry and an extreme case with maximum liner thickness, respectively.

The average projectile velocity recorded from three samples in Type 3 was approximately 2 096 m/s, while the velocity for Type 8 was measured at 1 783 m/s. These results confirm the trend predicted in simulation: the projectile formed from a moderately thick liner (Type 3) achieves a significantly higher speed than that from

a thicker liner (Type 8). The experimental velocities showed deviations of 6.6 % for Type 3 and 3.1 % for Type 8 compared to their respective simulation values, both within the acceptable error range of engineering applications.

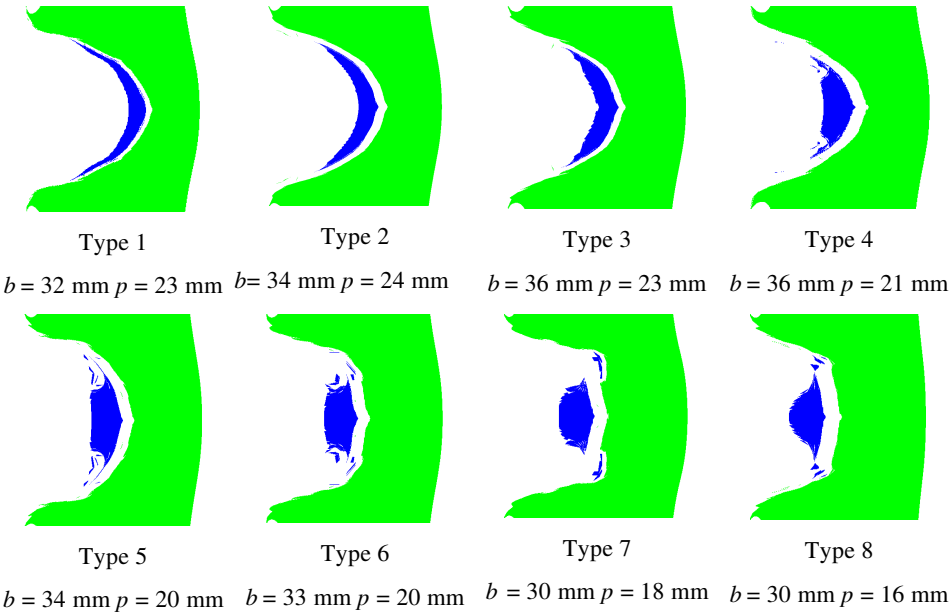

Fig. 8 EFP penetration process for different liner height

In terms of penetration performance, Type 3 demonstrated a wider and deeper penetration cavity. The average cavity width ($W_{h.Ag}$) was 37.7 mm, and the depth (D_h) ranged from 18 mm to 20 mm. In contrast, Type 8 produced a narrower and shallower cavity, with an average width of 26.3 mm and penetration depths between 14 mm and 17 mm. These differences underscore the importance of liner geometry: thinner-edged liners generate projectiles with better shape stability, higher energy delivery, and more effective target interaction.

Overall, the experimental results provide strong support for the simulation findings and further confirm that liner configurations with moderate thickness ratios, such as the one with a δ_2 to δ_1 ratio around 0.4, offer the most favorable balance between projectile velocity, flight stability, and terminal performance, as illustrated in Fig. 9.

5 Conclusions

This study investigated the effect of liner thickness distribution on EFP performance through simulations and experiments. Results showed that the edge-to-top thickness ratio (δ_2/δ_1) significantly affects projectile velocity, kinetic energy, shape stability, penetration depth, and cavity width.

Liners with low δ_2/δ_1 ratios tend to generate blunt, large-diameter EFPs with poor aerodynamic performance, leading to significant velocity loss during flight and limited penetration capability due to insufficient mass concentration. On the other hand, high δ_2/δ_1 ratios produce projectiles with slender, aerodynamically favorable shapes, but these designs often develop pronounced hollow tails that reduce flight stability and significantly reduce the EFP's penetration ability. The optimal performance is ob-

served at moderate δ_2/δ_1 ratios (approximately 0.4–0.6), where a balanced interaction between liner collapse dynamics, projectile geometry, and mass distribution results in superior velocity retention, stable flight, and enhanced penetration efficiency.

These findings highlight the importance of optimizing δ_2/δ_1 to enhance EFP efficiency. A well-balanced liner profile improves projectile stability, energy transfer, and target penetration, offering valuable guidance for warhead design.

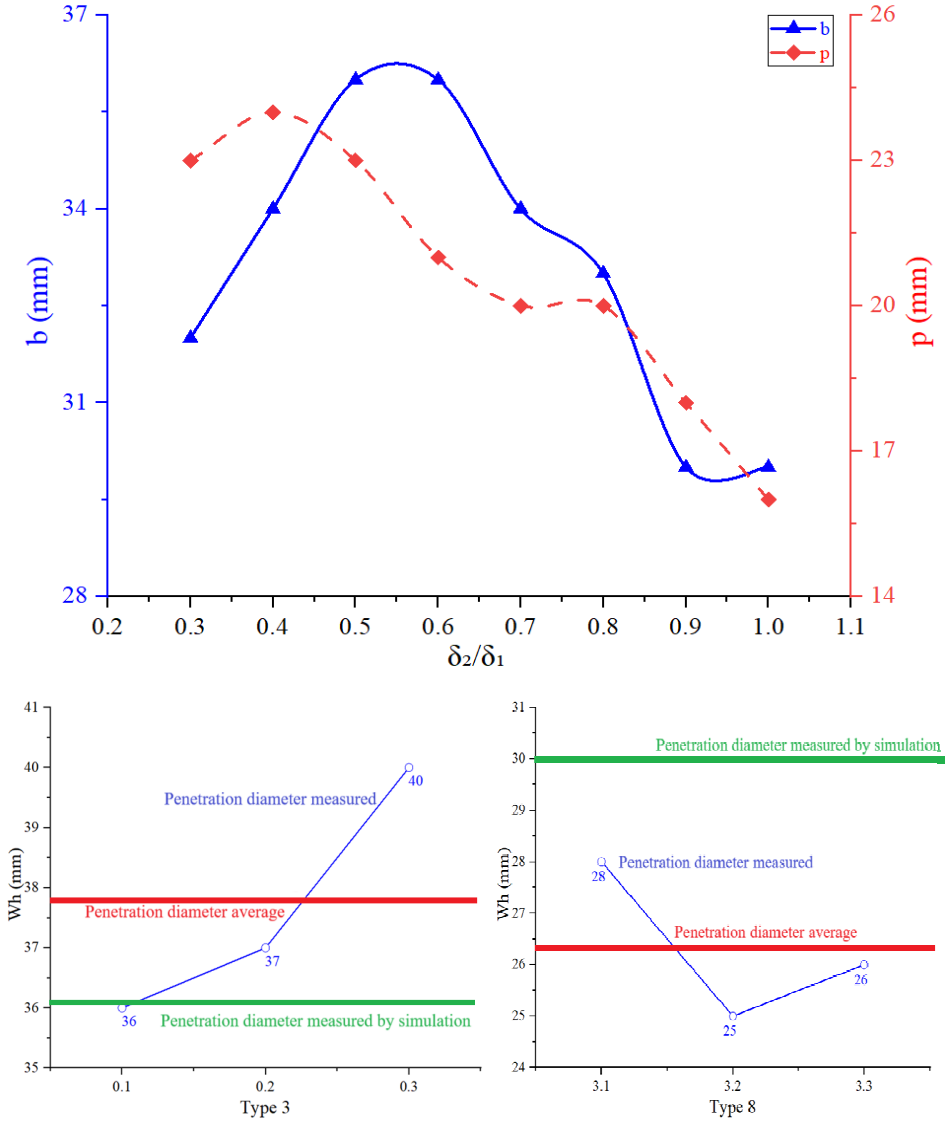

Fig. 9 Diameter and depth of EFP obtained by simulation and experiments

References

[1] ANDREEV, S.G., et al. *Physics of Explosion* (in Russian). 3rd ed. Moscow: Fizmatlit, 2004. ISBN 978-5-9221-0218-6.

[2] ORLENKO, L.P. *Physics of Explosion and Impact* (in Russian). 2nd ed. Moscow: Fizmatlit, 2008. ISBN 978-5-9221-0891-1.

[3] WU, J., J. LIU and Y. DU. Experimental and Numerical Study on the Flight and Penetration Properties of Explosively Formed Projectile. *International Journal of Impact Engineering,* 2007, **34**(7), pp. 1147-1162. DOI 10.1016/j.ijimpeng. 2006.06.007.

[4] SALKIČEVIĆ, M. Numerical Simulations of the Formation Behavior of Explosively Formed Projectiles. *Defense and Security Studies*, 2022, **3**, pp. 1-14. DOI 10.37868/dss. v3 .id183.

[5] CARDOSO, D. and F. TEIXEIRA-DIAS. Modelling the Formation of Explosively Formed Projectiles (EFP). *International Journal of Impact Engineering*, 2016, **93**, pp. 116-127. DOI 10.1016/j.ijimpeng.2016.02.014.

[6] YANG, D and J. LIN. Numerical Investigation on the Formation and Penetration Behavior of Explosively Formed Projectile (EFP) with Variable Thickness Liner. *Symmetry*, 2021, **13**(8), 1342. DOI 10.3390/sym13081342

[7] COUQUE, H. and R. BOULANGER. EFP Simulations with Johnson-Cook Models. In: *23rd International Symposium on Ballistics*. Tarragona: ISB, 2007, pp. 255-262.

[8] COUQUE, H., R. BOULANGER and F. BORNET. A Modified Johnson-Cook Model for Strain Rates Ranging from 10^3 to 10^5 s^{-1}. *Journal de Physique IV*, 2006, **134**, pp. 87-93. DOI 10.1051/jp4:2006134015.

[9] HUSSAIN, G., A. HAMEED, J.G. HETHERINGTON, P.C. BARTON and A.Q. MALIK. Hydrocode Simulation with Modified Johnson-Cook Model and Experimental Analysis of Explosively Formed Projectiles. *Journal of Energetic Materials*, 2013, **31**(2), pp. 143-155. DOI 10.1080/07370652.2011.606453.

[10] LI, B.Y., et al. Orthogonal Optimization Design and Experiments on Explosively Formed Projectiles with Fins. *International Journal of Impact Engineering*, 2023, **173**, 104462. DOI 10.1016/j.ijimpeng.2022.104462.

[11] LEE, E., M. FINGER and W. COLLINS. JWL Equation of State Coefficients for High Explosives [online]. 1973 [viewed 2025-10-12]. DOI 10.2172/4479737. Available from: https://www.osti.gov/servlets/purl/4479737

[12] JOHNSON, G.R. and W.H. COOK. Fracture Characteristics of Three Metals Subjected to Various Strains, Strain Rates, Temperatures and Pressures. *Engineering Fracture Mechanics*, 1985, **21**(1), pp. 31-48. DOI 10.1016/0013-7944(85)90052-9.

[13] *ANSYS Autodyn User's Manual* [online]. 2018 [viewed 2025-10-20]. Available from: https://www.scribd.com/document/453341462/ANSYS-Autodyn-Users-Manual-pdf

VAZIRI, M.R., M. SALIMI and M. MASHAYEKHI. A New Calibration Method for Ductile Fracture Models as Chip Separation Criteria in Machining. *Simulation Modelling Practice and Theory*, 2010, **18**(9), p. 1286-1296. DOI 10.1016/j.simpat.2010.05.003.